COLD FUSION CHANNELS OF $^{290}114$

R. A. GHERGHESCU

Horia Hulubei - National Institute for Nuclear Physics and Engineering,
P.O. Box MG-6, RO-76900, Bucharest, Romania, E-mail:rgherg@ifin.nipne.ro

Received June 9, 2005

Fusion reactions are calculated to synthesize $^{290}114$ elements. Potential energy surfaces are obtained as the result of dynamic minimization with independent deformations of the target and projectile, small semiaxis of the projectile and distance between centers as degrees of freedom. Binary macroscopic-microscopic method is used to obtain the deformation energy and Werner-Wheeler approximation yield the mass tensor. Charge asymmetry is varied for the same mass asymmetry channel belonging to an energy valley. The highest penetrability values are obtained for cold fusion channels within ^{104}Kr, ^{108}Sr and ^{112}Zr leading to $^{290}114$.

1. INTRODUCTION

In the synthesis of superheavy nuclei, the choice of the reaction channel and of the proper kinetic energy can lead to the best chance for compound nucleus formation. This work is devoted to the search of the optimal sub-barrier fusion channels towards $^{290}114$. Though it is known that cross section decreases with decreasing E_{CM}, the present calculations take advantage of obtaining the compound nucleus in the lowest excitation energy, close to its ground state. In this way it might be possible for the superheavy nucleus to be more stable against imediate alpha decay, cluster emission or fission. The main issue this work is supposed to study is the optimum fusion reaction for the lowest possible kinetic energy of the projectile. Choosing a neutron-richer isotope for example, as a projectile, has as a result a substantial change of the cross section [1]. Up to the complete fusion, the system may however be hindered to reach the final compound nucleus by quasi-fission, a situation taken into account in the dinuclear system model [2]. A valuable hint about mass-charge combinations in fusion reaction arouses from diffusion calculations [3] and obtaining the intermediate equilibrium N/Z values. For the exact isotopic composition of the optimal reaction, all possible isobaric combinations should be browsed for the same mass asymmetry. Best isotopic composition has been calculated for cold fusion reactions in [4], by getting the largest product between compound nucleus formation probability and a survival probability. The effect of interchanging neutrons within a given mass asymmetry channel is also studied using the

quantum molecular dynamics model [5]. Here isospin influence on the barrier lowering shows that neutron richer projectile enhances the fusion cross section against neutron-rich target, though the results are presented for intermediary mass (Ca+Zr) partners. Justification is given by the influence of N/Z changes in the neck-formed region, hence the study depends on the degree of overlapping as the neck develops. An increase of the neutron number of the target could increase the fusion cross section for light nuclei reactions [6]. For extreme sub-barrier reactions, like it is the case in the present work, fusion paths are obtained as dynamical minimization over the potential energy surfaces. Potential energy surface studies have been also performed within the framework of self-consistent nuclear models like Skyrme-Hartree-Fock and relativistic mean field [7, 8]. It is shown by these authors that shell closures lower the fusion barrier for a given (A_P, Z_P), (A_T, Z_T) pair, if one supposes cold fusion reactions. The same closure effect is stressed also in a cluster emission type calculation [9].

There are a lot of factors that can hinder fusion and consequently make sub-barrier fusion cross section to be overestimated if only synthesis is reckoned. Rates of fusion obtained from penetrability could be improved by taking into account friction under the barrier [10] or quasifission [3]. Since isobaric reactions for superheavy production are to be studied here, one should mention that, due to the necessity of using neutron-rich partners, possible neutron transfer could take place between nuclei [11].

Potential energy surfaces usually exhibit valleys interpreted as advantageous paths toward complete fusion. Such minimum sequences in deformation energy start at a certain mass asymmetry. In order to obtain the optimal pair (A_T, Z_T), (A_P, Z_P), an $\eta_A = (A_T - A_P)/A$ -path must be browsed in Z-direction and this is achieved by exhausting all possible isobaric reactions in a η_A-minimum energy channel. The present work studies the sub-barrier fusion reactions leading to the synthesis of $^{290}114$. The macroscopic-microscopic method is employed, within the subsequent steps: calculation of the deformation energy using independent intermediary spheroidal deformations of the target and projectile ($\chi_T = b_T/a_T$, $\chi_P = b_P/a_P$), where (b_T, a_T) and (b_P, a_P) are spheroid semiaxes, the small semiaxis of the projectile b_P and the distance between center R during the overlapping stage as degrees of freedom. This first part of the approach will be applied for the whole range of mass asymmetry (A_T, A_P) combinations, choosing (Z_T, Z_P) as the one with the lowest value of total deformation energy for separated target and projectile. The *static* barriers for these pairs are obtained by energy minimization over the multidimensional space of deformation. The second stage of the approach is the repetition of the calculation for all possible isobaric reaction channels inside the promising valleys obtained at the first stage. Final stage is the dynamical calculation. The mass tensor is calculated by means

of Werner-Wheeler irrotational flow method. The action integral is then computed for all isobaric reactions with the lowest static barriers. Minimization of the action integral within the 4-dimensional space of deformation will provide the final penetrability value for every cold fusion channel.

Section 2 is a brief presentation of the deformation energy calculation. Section 3 describes the mass tensor components and the dynamical minimization of the action integral. Section 4 is devoted to the results and discussion.

2. TOTAL DEFORMATION ENERGY

Only head-on configurations for two intersected spheroids are calculated. A binary macroscopic-microscopic method is used to calculate the deformation energy. Single particle energy levels are obtained by the deformed two-center shell model. Details of calculation are given in [12]. In the Schrödinger equation:

$$H\Psi - E\Psi = 0 \tag{1}$$

the total Hamiltonian:

$$H = -\frac{\hbar}{2m_0}\Delta + V(\rho, z) + V_{\Omega s} + V_{\Omega^2} \tag{2}$$

is deformation dependent. The deformed two-center oscillator potential for target and projectile regions v_T and v_P reads:

$$V(\rho, z) = \begin{cases} V_T(\rho, z) = \frac{1}{2}m_0\omega_{\rho_T}^2\rho^2 + \frac{1}{2}m_0\omega_{z_T}^2(z + z_T)^2, \text{ for } v_T \\ V_P(\rho, z) = \frac{1}{2}m_0\omega_{\rho_P}^2\rho^2 + \frac{1}{2}m_0\omega_{z_P}^2(z - z_P)^2, \text{ for } v_P \end{cases} \tag{3}$$

where z_T and z_P are the centers of the target and projectile, and equality:

$$V_T(\rho, z) = V_P(\rho, z) \tag{4}$$

defines the border between v_T and v_P regions; the relation with the deformations of the two spheroid semiaxes (b_i, a_i) is given by the frequency relations:

$$\begin{aligned} m_0\omega_{\rho_i}^2 &= (a_i/b_i)^{2/3} \cdot m_0\omega_{0i}^2 = (a_i/b_i)^{2/3} \cdot 54.5/R_i^2 \\ m_0\omega_{zi}^2 &= (b_i/a_i)^{4/3} \cdot m_0\omega_{0i}^2 = (b_i/a_i)^{4/3} \cdot 54.5/R_i^2 \end{aligned} \tag{5}$$

where $R_i = r_0A_i^{1/3}$, and b_i, a_i are the spheroid semiaxes.

Since the angular momentum dependent potentials $V_{\Omega s}$ and V_{Ω^2} depend on $\nabla V(\rho, z)$, these terms also follow any changes in the deformation of the partially overlapped fragments. Another deformation-dependent factor is the spin-orbit

interaction strength. Its value determines the shell closures for different nuclear mass regions. Since the heavy and light fragment action manifests itself within space regions defined by eq. (4), change of the spin-orbit strength parameter from target to projectile is effectuated within space regions depending on the two semiaxis ratios $\chi_T = b_T/a_T$ and $\chi_P = b_P/a_P$. Usual matrix diagonalization of H leads to the level scheme of two partially overlapped spheroids for a given distance R between centers and intermediary (independent) χ_T and χ_P. The sequence of level schemes is used in the Strutinsky method [13] to compute separately the proton and neutron shell corrections. This is a very important point of the calculation, especially when one aims to cold fusion of superheavy nuclei. It is well known that these nuclei survive only due to negative shell corrections, their macroscopic barrier being negligible [14]. At certain intermediary deformations (χ_T and χ_P at given R), partially overlapped shells display proton and/or neutron closure and minima are generated in the shell corrections. These minima substantially contribute to the energy valleys.

The macroscopic part is computed with the Yukawa-plus-exponential model. As a peculiarity, the Coulomb E_C [16] and the nuclear surface term E_Y [17] are computed as:

$$E_C = \frac{2\pi}{3}(\rho_{eT}^2 F_{C_T} + \rho_{eP}^2 F_{C_P} + 2\rho_{eT}\rho_{eP} F_{C_{TP}}) \tag{6}$$

and

$$E_Y = \frac{1}{4\pi r_0^2}[c_{sT} F_{EYT} + c_{sP} F_{EY_P} + 2(c_{sT} c_{sP})^{1/2} F_{EY_{TP}}] \tag{7}$$

where ρ_{ei} is the charge density and c_{si} the surface coefficient. F_{C_i} and F_{EY_i} are shape dependent integrals. The last term in paranthesis is the Coulomb and respectively nuclear surface interaction between target and projectile within overlapping [18]. Both E_C and E_Y are in that way deformation dependent. The total deformation energy E_{def} is obtained as:

$$E_{def} = E_{macro} + E_{shell} \tag{8}$$

where:

$$E_{macro} = (E_C - E_C^{(0)}) + (E_Y - E_Y^{(0)}) \tag{9}$$

scaled to the sphere values $E_C^{(0)}$ and $E_Y^{(0)}$ and E_{shell} is the shell correction energy.

3. MASS TENSOR AND PENETRABILITY

There are four independent variables describing the configuration of two intersected spheroids: the ratios of the spheroid semiaxes for target χ_T and

projectile χ_P, the small semiaxis of the projectile b_P (the target semiaxis b_T results from volume conservation) and the distance between centers R. From Werner-Wheeler approach [19], the main term reads:

$$B'_{ij} = \int_{z_m}^{z_M} T_{ij}(z;q)\,\mathrm{d}z \tag{10}$$

with:

$$T_{ij} = \rho_s^2(z)\left[X_i X_j + \frac{1}{8}\rho_s^2(z)\frac{\partial X_i}{\partial z}\frac{\partial X_j}{\partial z} \right] \tag{11}$$

where i, j are one of the four deformation coordinates and:

$$X_i(z) = \frac{1}{\rho_s^2(z;q)}\frac{\partial}{\partial q_i}\int_z^{z_M} \rho_s^2(z';q)\mathrm{d}z' \tag{12}$$

where $\rho_s(z)$ describes the surface. A second term in the tensor component is responsible for the correction due to the center of mass motion. It has been calculated here starting from the kinetic energy expression, with discrete velocities of the type $\left(\dot{\vec{r}}'_i - \dot{\vec{R}}_{CM}\right)$, and convert the sums into integrals over the whole binary shape configuration. The mass tensor correction components are obtained as:

$$B^c_{ij} = \frac{\sigma_m^2\pi^2}{M}\left\{\left[\int_{z_m}^{z_M} \rho_s^2(z)X_i(z)\mathrm{d}z\right]\left[\int_{z_m}^{z_M} \rho_s^2(z')X_j(z')\mathrm{d}z'\right]\right\}$$

where M is the total mass of the system. Finally, the total components of the inertial mass tensor are calculated as:

$$B_{ij} = B'_{ij} - B^c_{ij} \tag{13}$$

In order to perform the further action integrals, it is useful to contract the tensor along one of the coordinates. A first condition in the numerical computation is to impose the projectile volume to decrease by a fixed amount $\Delta V_P = 0.15V_P$ (arbitrary) at every step value R, as the projectile enters the target. Second, one complies to the variation law of χ_T and χ_P such that at the touching point (start of the process) they take initial (separated nuclei) values χ_{T0} and χ_{P0}. At the end χ_T must be equal to the compound nucleus value χ_0, while χ_P ends at an independent χ_{Pf}. There are obviously many functions to describe such a pass. This work proposes a simple linear transition:

$$\chi_T = \chi_{T0} + (\chi_0 - \chi_{T0})\frac{R - R_f}{R_t - R_f}\frac{100}{k_T}$$

$$\chi_P = \chi_{P0} + (\chi_{Pf} - \chi_{P0}) \frac{R - R_f}{R_t - R_f} \frac{100}{k_P} \tag{14}$$

if $R < 0.01(R_t - R_f)k_T$ for χ_T and $R < 0.01(R_t - R_f)k_P$ for χ_P. k_T and k_P are an independent number of steps in R direction with $k_T,\ k_P < 100,$ and oblige the number of steps (or the distance range in R) along which the semiaxis ratios change. Also:

$$\chi_{Pf} = \chi_{P0} - \frac{i_P}{10}(\chi_0 - \chi_{P0}) \tag{15}$$

introduces i_P as another independent parameter, which describes how much the projectile changed its initial semiaxis ratio along the overlapping process. Due to eqs. (14) and (15), χ_T, χ_P and b_P are independent degrees of freedom. Possible transition paths for χ_T and χ_P are thus displayed in Fig. 1, for different k_T, k_P.

The horizontal part of the plot, lines starting from R_t, measures for how long the target and/or projectile (lower plot) preserve their initial semiaxis ratio. In

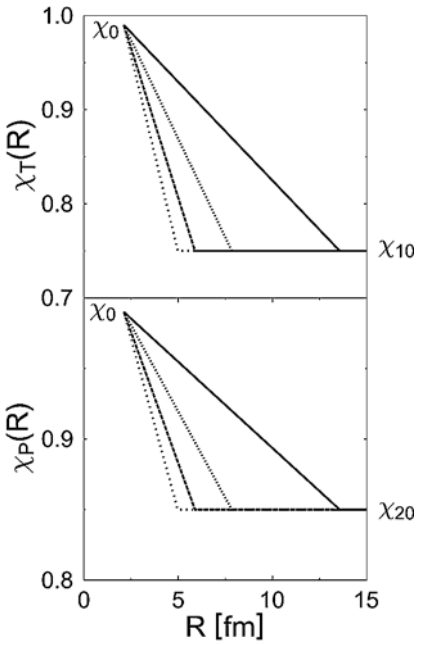

Fig. 1. – Different paths of variation for the semiaxis ratios of the target (χ_T) and projectile (χ_P) as a function of the distance between centers R.

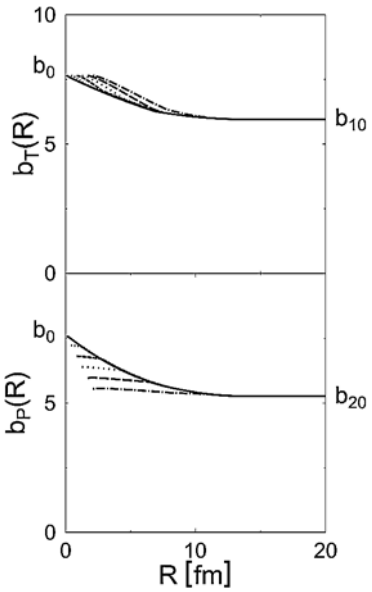

Fig. 2. – Different paths of variation for the small semiaxis of the target (b_T) and projectile (b_P) as a function of R.

these plots, both partners end at the compound nucleus value $\chi_{Tf} = \chi_0$ and $\chi_{P0} = \chi_0$. The lines differ by k_T (upper plot) and k_P respectively. Fig. 2 shows different paths of the target (b_T, upper plot) and projectile (b_P) small semiaxes, for the same values of k_T, k_P and i_P as in Fig. 1.

In all cases b_T ends at the same value b_0 of the final compound nucleus semiaxis. For b_P conditions are more relaxed. The dashed-dotted horizontal line for b_P represents the case when the projectile does not change its shape and dimensions all along the overlapping process. These considerations lead to the dependence of b_P, χ_T and χ_P on the same parameters:

$$\begin{aligned} b_P &= b_P(k_T, k_P, i_P; R) \\ \chi_T &= \chi_T(k_T, k_P, i_P; R) \\ \chi_P &= \chi_P(k_T, k_P, i_P; R) \end{aligned} \tag{16}$$

The number of steps k_T, k_P and i_P are varied numerically within such range that $b_0 > b_P \geq b_{P0}$ and $\chi_T \in (\chi_0, \chi_{T0})$ and $\chi_P \in (\chi_{Pf}, \chi_{P0})$. The above functions allow to obtain numerically the derivatives to R. Final contracted total mass inertia becomes:

$$\begin{aligned} B(R) = {} & B_{b_P b_P}\left(\frac{\mathrm{d}b_P}{\mathrm{d}R}\right)^2 + 2B_{b_P\chi_T}\frac{\mathrm{d}b_P}{\mathrm{d}R}\frac{\mathrm{d}\chi_T}{\mathrm{d}R} + 2B_{b_P\chi_P}\frac{\mathrm{d}b_P}{\mathrm{d}R}\frac{\mathrm{d}\chi_P}{\mathrm{d}R} + \\ & + 2B_{b_P R}\frac{\mathrm{d}b_P}{\mathrm{d}R} + B_{\chi_T\chi_T}\left(\frac{\mathrm{d}\chi_T}{\mathrm{d}R}\right)^2 + 2B_{\chi_T\chi_P}\frac{\mathrm{d}\chi_T}{\mathrm{d}R}\frac{\mathrm{d}\chi_P}{\mathrm{d}R} + \\ & + 2B_{\chi_T R}\frac{\mathrm{d}\chi_T}{\mathrm{d}R} + B_{\chi_P\chi_P}\left(\frac{\mathrm{d}\chi_P}{\mathrm{d}R}\right)^2 + 2B_{\chi_P R}\frac{\mathrm{d}\chi_P}{\mathrm{d}R} + B_{RR} \end{aligned} \tag{17}$$

It is important to emphasize that the above laws of variation restrict by no means the system to follow a certain path. The final fusion path is obtained as the result of minimization over *all* the possible values (hence all range of κ_T, κ_P, i_P) in *any* direction at a fixed R. Thus, when the action integral is minimized, the configuration follows an energy valley which is not necessary along one of the variation laws indicated above. The system simply can switch from one set of (κ_T, κ_P, i_P) to another set ((κ'_T, κ'_P, i'_P) at successive R-steps.

Penetrability P for a given fusion path is calculated as usual:

$$P = \exp(-K_{ov}) \tag{18}$$

where K_{ov} is the overlapping action integral. The barriers are supposed to be tunneled at the level of the final compound nucleus ground state. This is the

minimum value of the kinetic energy in this work where sub-barrier fusion reactions are intended to take place at the lowest energy. K_{ov} is calculated numerically as:

$$K_{ov}(b_P, \kappa_T, \kappa_P; R) = \frac{2}{\hbar}\int_{(fus)} [2B(R)_{b_P,\kappa_T,\kappa_P} E_{def}(R)_{b_P,\kappa_T,\kappa_P}]^{1/2} \mathrm{d}R \qquad (19)$$

Since K_{ov} is calculated for every set $(b_P, \kappa_T, \kappa_P)$ at every point R, the penetrability presents itself as a multidimensional lot. The final value of P for every channel reaction is the result of action integral K_{ov} minimization over the whole range of $(b_P,\ \kappa_T,\ \kappa_P,\ R)$.

4. RESULTS AND DISCUSSION

The deformation energy is computed for every possible $(A_T,\ A_P)$ fusion channel leading to the same compound nucleus. Calculations are performed for ^{290}114. Mass asymmetries start from $\eta_A = 0$ with symmetric reaction ^{144}Ba+^{146}Ce up to $\eta_A \simeq 0.84$ corresponding to ^{24}Mg+^{266}No. A very pronounced valley is visible at $\eta_A \simeq 0.31$, around ^{104}Kr+^{186}Pt with a barrier height at 7.22 MeV. The barrier entrance point is situated deep in the overlapping region compared to more asymmetric reactions. Lead target (^{82}Ge+^{208}Pb) reaction, corresponding to $\eta_A \simeq 0.46$, has a barrier height of 12.21 MeV, though it takes advantage of two neutron and one proton shell closures. It is a direct proof that having magic or double magic partners does not mean the lowest barrier is granted. Moreover, since the action integral is calculated along the whole fusion path (*fus*) – eq. (19), the width becomes also important, and one can observe how much the asymmetric channel is favored. A particular trend has been obtained in successive reactions using projectiles ^{80,84,88,92}Ge. The calculated barriers decrease monotonously as E_{def} : 14.84, 11.26, 8.90, 8.18 MeV respectively. It is a behaviour which has been analyzed in detail for a lighter sequence of Ge isotopes, also displaying constant increase of deformation in [22], where a very complete coupled channel analysis is made about the effect of deformation on fusion cross section (measured cross sections in this article were higher for neutron-richer Ge isotopes, maybe favoring a lower fusion barrier as deformation increases).

The action integral has been minimized for $(A_T,\ A_P)$ between (168, 122) and (190, 100), browsing the energy valley around $\eta_A \simeq 0.3$. Isobaric reactions with all obtainable (stable) partners are subjected to calculation in order to reveal first the isospin influence within the same η_A and then to obtain the maximum penetrability.

The resulted penetrabilities are presented in Table 1, for $^{290}114$ There are small differences between barriers, all being around 7–8 MeV, the average height of the energy valley. On the contrary, penetrabilities display very large differences. The most favorable values are obtained for (^{104}Kr+^{186}Pt), with $\log_{10}P = -7.25$, (^{108}Sr+^{182}W) with $\log_{10}P = -8.036$ and (^{112}Zr+^{178}W) with $\log_{10}P = -8.664$. These reactions have also the lowest barrier height, but variations against, for example (^{104}Sr+^{186}Os) with $E_b = 7.52$ MeV and $\log_{10}P = -12.233$ or (^{112}Mo+^{178}Hf) with $E_b = 7.77$ MeV and $\log_{10}P = -10.823$ are not at all linearly dependent on Z or A. Despite just a small barrier height difference, the width of the barrier together with the dynamic influence of the mass tensor play a major role. ^{110}Ru+^{180}Yb is only 2 neutron poorer in target and projectile compared to ^{112}Zr reaction, and yet it produces the lowest penetrability value, $\log_{10}P = -23.688$. Its barrier is not very high, but the width is probably the largest. It is also interesting to compare this unfavorable reaction with its isobaric, ^{110}Mo+^{180}Hf. However, this is a weak point of the present approach: oblate deformations cannot be taken into account, and Ru isotopes have very negative β_2 values. Here, a rough approximation has been made, by taking these oblate nuclei as spherical.

Table 1

The dynamic barriers E_b and logarithms of penetrabilities $\log_{10}P$ for the energy valley in synthesis of $^{290}114$

Reaction	E_b [MeV]	$\log_{10}P$
^{104}Kr+^{186}Pt	7.22	–7.250
^{104}Sr+^{186}Os	7.52	–12.233
^{104}Zr+^{186}W	7.75	–14.353
^{104}Mo+^{186}Hf	8.08	–16.106
^{106}Zr+^{184}W	7.66	–12.976
^{106}Mo+^{184}Hf	7.93	–12.956
^{108}Sr+^{182}Os	7.37	–8.036
^{108}Zr+^{182}W	7.62	–11.245
^{108}Mo+^{182}Hf	7.91	–12.892
^{110}Mo+^{180}Hf	7.85	–11.688
^{110}Ru+^{180}Yb	9.01	–23.688
^{112}Zr+^{178}W	7.33	–8.664
^{112}Mo+^{178}Hf	7.77	–10.823
^{112}Ru+^{178}Yb	8.73	–20.162
^{114}Mo+^{176}Hf	8.12	–15.690
^{114}Ru+^{176}Yb	8.45	–18.747

As a final remarque, one states that the extreme sub-barrier fusion as an alternative to high energy synthesis reaction has certainly the disadvantage of having a very low probability, hence a low cross section. However, the final compound nucleus could be synthesized in a more stable state (no excitation), thus it probably lives longer. Within the presented adiabatic approach, the three favorable reactions mentioned above do have a rather high penetrability value for cold fusion, and could be used for such experiments to synthesize $^{290}114$. None of the reactions took advantage of proton and/or neutron magicity.

5. CONCLUSIONS

When nuclei approach to each other with a kinetic energy equal to the Q-value of the reaction, chances are to obtain a compound nucleus very close to its ground state. Since no excitation triggers a decay process, the final system could be more stable and live longer. The space of deformation that has been used to obtain the results of this work includes a complete number of parameters to describe head-on collisions of spheroidally deformed partners. Different semiaxis ratios of the target and projectile during the overlapping region and variable projectile semiaxis b_P insure new degrees of freedom in the microscopical shell level calculation, and finally in obtaining the total deformation energy and mass tensor. The present approach used a binary model to study the dynamics of possible sub-barrier fusion reactions towards the synthesis of two superheavy isotopes.

$^{290}114$ has chances to be obtained by extreme sub-barrier fusion, according to this work. It is demonstrated that only height of the barrier is not enough to judge on the total cross section. These reactions, obtained after browsing the deepest energy valley of (E_{def}, η_A, R) produced narrow barriers and much larger penetrability values. ^{104}Kr+^{186}Pt, ^{108}Sr+^{182}Os and ^{112}Zr+^{178}W could be used in a trial experiment, to obtain $^{290}114$ in a close to ground state energy, by using a kinetic energy equal to the Q-value.

REFERENCES

1. S. Hofmann and G. Münzenberg, Rev. Mod. Phys., **72**, 733 (2000).
2. N. V. Antonenko, E. A. Cherepanov, A. K. Nasirov, V. P. Permjakov and V. V. Volkov, Phys. Rev., **C51**, 2635 (1995).
3. G. G. Adamian, N. V. Antonenko and W. Scheid, Phys. Rev., **C68**, 034601 (2003).
4. G. G. Adamian, N. V. Antonenko and W. Scheid, Phys. Rev., **C69**, 011601(R) (2004).
5. Ning Wang, Xizhen Wu and Zhuxia Li, Phys. Rev., **C67**, 024604 (2003).
6. K. Satou, H. Ikezoe, S. Mitsuoka, K. Nishio and S. C. Jeong, Phys. Rev., **C65**, 054602 (2002).
7. M. Bender, K. Rutz, P-G. Reinhard, J. A. Maruhn and W. Greiner, Phys. Rev., **C58**, 2126 (1998).

8. J. F. Berger *et al.*, Nucl. Phys., **A685**, 1 (2001).
9. M. Goncalves and S. B. Duarte, Phys. Rev., **C48**, 2409 (1993).
10. B. G. Giraud, S. Karataglidis, K. Amos and B. A. Robson, Phys. Rev., **C69**, 064613 (2004).
11. V. I. Zagrebaev, Phys. Rev., **C67**, 061601(R) (2003).
12. R. A. Gherghescu, Phys. Rev., **C67**, 014309 (2003).
13. V. Strutinsky, Nucl. Phys., **A95**, 420 (1967).
14. A. Sobiczewski, Phys. Part. Nucl., **25**, 295 (1994).
15. Z. Patyk and A. Sobiczewski, Phys. Lett., **B256**, 307 (1991).
16. K. T. Davies and A. J. Sierk, J. Comp. Phys., **18**, 311 (1975).
17. H. J. Krappe, J. R. Nix and A. J. Sierk, Phys. Rev., **C20**, 992 (1979).
18. D. N. Poenaru, M. Ivascu and D. Mazilu, Comp. Phys. Comm., **19**, 205 (1980).
19. K. T. Davies, A. J. Sierk and J. R. Nix, Phys. Rev., **C13**, 2385 (1976).
20. R. A. Gherghescu, J. Skalski, Z. Patyk and A. Sobiczewski, Nucl. Phys., **A651**, 237 (1999).
21. P. Möller, J. R. Nix and K-L. Kratz, At. Data Nucl. Data Tables, **66**, 131 (1997).
22. H. Esbensen, Phys. Rev., **C68**, 034604 (2003).